Int J Adv Manuf Technol (2010) 46:411–421
DOI 10.1007/s00170-009-2103-y

ORIGINAL ARTICLE

# A new generalized upper-bound solution for the ECAE process

**K. Abrinia · M. J. Mirnia**

Received: 15 November 2008 / Accepted: 7 May 2009 / Published online: 31 May 2009


**Abstract** A new generalized upper-bound solution for the equal-channel angular extrusion (ECAE) process is presented in this paper. Using mathematical definition of Bezier curves, a streamline was formulated to define a generalized deforming region. Based on this deforming region, a kinematically admissible velocity field was obtained from which upper-bound solutions were computed. By changing the parameters defining the Bezier-shaped streamline which in turn defines the deforming region, the optimization of the upper-bound solution was carried out. Equal-channel angular extrusion through a 90° bend was considered. Using the formulation presented in here, it was possible to predict the shape of the dead metal zone and its variation with frictional conditions. Unlike previous work in which a fixed circular shape had been assumed for the dead metal zone, in this paper, a generalized shaped Bezier curve was used. The optimum value of the extrusion pressure for ECAE was obtained and compared with both experimental and theoretical data from previous works. It was concluded that the present solution gave an improvement over all previous works and the authors' results were closer to experimental data.

**Keywords** ECAE · Upper bound · Velocity field · Bezier curves · Dead metal zone

**Nomenclature**

| | |
|---|---|
| $x_i$,$y_i$ | The coordinate of point $p_i$ defining Bezier characteristic polygon |
| $\psi$, $\psi_1$, $\psi_2$, and $\psi_3$ | Angles shown in Fig. 2 |
| $\nu$, $w$, and $r$ | Parameters used for optimizing upper-bound solution |
| $a$, $b$, and $h$ | Parameters defining die geometry shown in Fig. 2 |
| $\phi$ | Die bend angle |
| $\nu_0$ | Velocity of material in zones I and IV |
| $t$ | Parameter determining the position of the particle on a streamline |
| $u$ | Parameter determining the position of the particle on channel width |
| $X$,$Y$ | Coordinates of a particle in the deforming zone or the parametric co-ordinate of Bezier curves |
| $\nu_x$,$\nu_y$ | Components of velocity field |
| $\dot{\varepsilon}_x$,$\dot{\varepsilon}_y$, and $\dot{\tau}_{xy}$ | Components of strain rate in deforming zone |
| $\dot{W}$ | Power dissipated during the process |
| $F$ | Force applied during the process |
| $\bar{y}_0$, $y_0$ | Average yield stress, the yield stress |
| $m$ | Friction constant |
| $\alpha$ | Acute angle between the tangent of streamline and the y axis |
| $\varepsilon_{ave}$ | Total equivalent strain induced during process |
| $\varepsilon_{stream}$ | Equivalent strain induced in deforming zone |
| $\varepsilon_{si}$, $\varepsilon_{so}$, and $\varepsilon_s$ | Equivalent strains induced in entry and exit discontinuity surfaces, sum of $\varepsilon_{si}$ and $\varepsilon_{so}$ |
| $\gamma_i$ and $\gamma_o$ | Shear strains induced in entry and exit discontinuity surfaces |
| $\lvert\Delta v\rvert$ | Velocity discontinuity |
| $l_i$,$l_o$ | Instant length of the specimen in the entry and exit channel before point A and after point B |

K. Abrinia (✉) · M. J. Mirnia
Mechanical Engineering Department, College of Engineering, University of Tehran,
Tehran, Islamic Republic of Iran
e-mail: Cabrinia@ut.ac.ir

| | |
|---|---|
| $v_{d0}$ | Initial velocity in deforming region on the entry discontinuity surface |
| $C$ | Constant for the velocity field equations to be determined from the boundary conditions |

## 1 Introduction

In recent years, materials and products with micro and nanosize grains have attracted a lot of attention, and researchers have tried to come up with new and effective solutions. Equal-channel angular extrusion has been the center of activities in this respect. In this process, usually, the material does not undergo any reduction of area, but the grain size is reduced due to the deformation through the angular movement in the extrusion die.

Altan et al [1] analyzed the deformation of the material during a 90° equal-channel angular extrusion (ECAE) process using upper-bound theorem. They suggested a model which included the effect of friction between the sample and the die walls, radius of inner corner of the die, and the dead metal zone on the deformation patterns during ECAE.

Eivani and Karimi Taheri [2] analyzed deformation of material in ECAE process with outer curved corner using an upper-bound solution. They considered the effects of die angle, friction between the sample and the die walls, and the angle of the outer curved corner on the extrusion pressure. Sandim et al. [3] deformed Niobium single crystals by ECAE with one, four, and eight passes at room temperature. They found that the microstructure of the sample deformed after one ECAE pass and displayed uniformly spaced coarse parallel sets of shear bands. In the most deformed specimen (eight ECAE passes), the microstructure was observed to be more uniform and consisted of fine grains with sizes of about 1 μm. Li et al. [4] investigated the microstructure and texture evolution in interstitial-free steel during ECAE using a 120° die for up to four passes via three routes. They used finite element simulation to help understand deformation behavior and texture formation. It was found that the efficiency of grain refinement was to be only mildly dependent on die angle and processing route. Zhang et al. [5] simulated the plastic deformation of commercially pure titanium by multi-pass ECAE, at medium hot working temperature, using finite element method. They found that unlike the single ECAE pass where the corner gap was important, it was the repetitive billet end side shift of less-deformed billet ends which were responsible for the development of the non-uniformly deformed zone in the multi-pass ECAE process. Tham et al. [6] conducted an experimental study on multi-pass ECAE process of a widely used aluminum 6061 alloy. They found out that there was a significant increase in the strain hardening exponent of the samples subjected to the different heat treatment configurations due to severe plastic deformation after multi-pass ECAE. Petryk and Stupkiewicz [7] studied the effect of severe plastic deformation (SPD) on grain refinement and strain hardening in polycrystalline metals. The decrease in size of dislocation cells and cell blocks was expressed as a function of the effective plastic strain influenced by strain rate reversals. The proposed model was claimed to provide a tool for quantitative comparison of different SPD processes. Kecskes et al. [8] presented two general methodologies for the production of ultrafine-grained (UFG) and nanocrystalline (NC) tungsten (W) metal samples, namely, the top-down and bottom-up. They used ECAE coupled with rolling to fabricate UFG W. They also conducted a series of bottom-up experiments to consolidate powdered UFG W precursors into solid bodies. The bottom-up approach relied on rapid, high-temperature consolidation specifically designed for UFG and NCW powders.

Su et al. [9] investigated the AZ31 Mg alloy samples processed by the ECAP process at 200°C for up to four passes. They studied the microstructural evolution during ECAP using optical microscope and transmission electron microscope. They proposed a model for the grain refinement mechanism of Mg during ECAP using data observed from the microstructure analysis. Hasani et al. [10] analyzed the flow lines in aluminum alloy 6061 during ECAE in a 90° die with and without the application of back pressure during pressing. They showed that back pressure slightly lowers the total strain, strongly increases the size of the plastic zone, and significantly reduces the plastic strain rate. Eivani and Karimi Taheri [11] studied the deformation of material during ECAE using an upper-bound model. They considered the effect of die angle and friction between the sample and the die walls on the geometry of dead metal zone and total strain. The relationship between the friction coefficient, the extent of dead metal zone, and total strain was derived.

A new formulation is presented in this paper for the ECAE process which uses a Bezier-shaped curve to define a general streamline. The deforming region is defined and optimized to minimize the upper-bound on the extrusion pressure.

## 2 Theory

The geometry of the ECAE die is shown in Fig. 1. The parameters defining the deforming geometry are illustrated in Fig. 2. Plane strain deformation has been assumed for the theoretical analysis presented here. In this geometry, the

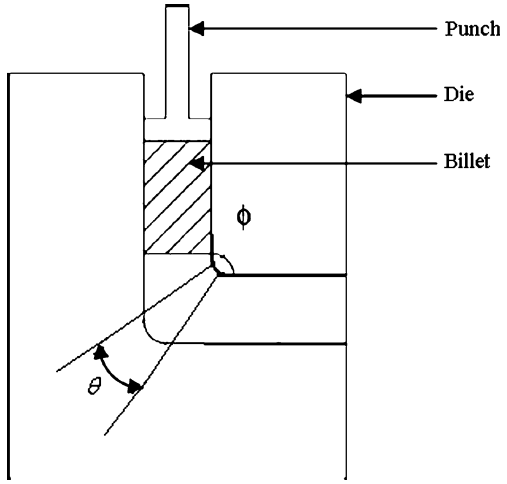


**Fig. 1** Die geometry for the ECAE process through a 90° bend

inner corner of the ECAE die (arc *D′C″E′*) has been assumed to be defined by a Bezier curve. The outer surface of the die has a sharp corner (point C), and hence, the material during deformation forms a dead metal zone in this area. The interface of the dead metal zone and the deforming region is defined by a streamline in the shape of a third-degree Bezier curve. All streamlines in the deforming regions are in fact symmetric with respect to line OC. Referring to Fig. 2, the size of the streamline diminishes as one moves from the interface of the dead metal zone towards the inner corner of the die. Therefore, by defining a particle moving on a general streamline, all points in the deforming region are defined.

In the present analysis, four distinct regions have been defined in the ECAE: region I where the material moves in a rigid manner before coming into contact with line OD where the deformation begins; region II defined by the boundaries *D′DEE′G′C′F′D′* which is the deforming zone; region III between lines DCE and arc DE which forms the dead metal zone; and, finally, region IV where the material after leaving the deforming region at line OE moves as a rigid body.

As mentioned earlier, the deforming region in this analysis has been formulated by a single equation defining a Bezier curve. Mathematically, for $n+1$ control points, the Bezier curve is defined by the following polynomial with $n$ degrees:

$$P(t) = \sum_{i=0}^{n} P_i B_{i,n}(t) \qquad 0 \le t \le 1 \tag{1}$$

where $P(t)$ is any point on the curve and $P_i$ is a control point. $B_{i,n}$ are the Bernstein polynomials:

$$B_{i,n}(t) = D(n,i)t^i(1-t)^{n-i} \tag{2}$$

where $D(n,i)$ is:

$$D(n,i) = \frac{n!}{i!(n-i)!}. \tag{3}$$

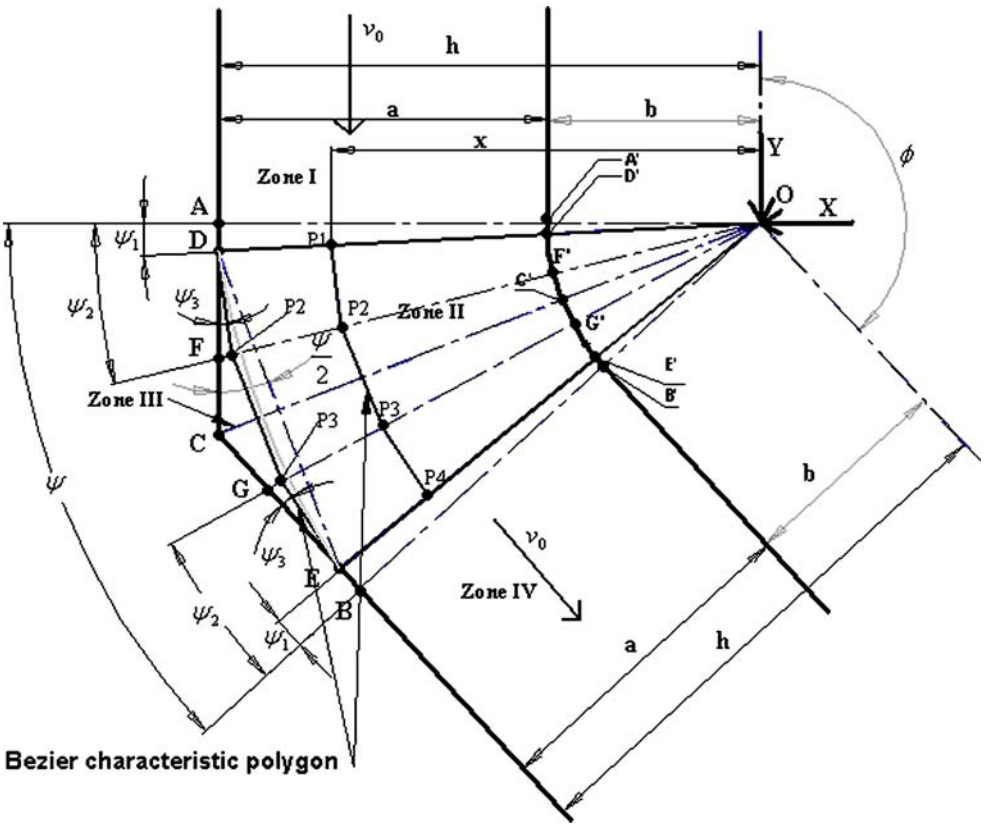


**Fig. 2** Geometry of deforming zone for the ECAE process through an arbitrary bend angle

Therefore, a Bezier curve with four control points as used in this paper can be expressed as follows:

$$P(t) = P_0(1-t)^3 + 3P_1t(1-t)^2 + 3P_2t^2(1-t) + P_3t^3 \quad 0 \le t \le 1. \tag{4}$$

To define such curves, consider a particle at a distance $x$ from point O (Fig. 2), moving on a streamline. Points $P_1$, $P_2$, $P_3$, and $P_4$ in Fig. 2 define the characteristics of a Bezier curve. The coordinates of these points ($x_1$, $y_1$, $x_2$, $y_2$, $x_3$, $y_3$, $x_4$, and $y_4$) are defined as follows:Defining the line $p_1p_2$ (Fig. 2), we have:

$$y - y_1 = -(\cot\psi_3)(x - x_1). \tag{5}$$

Line OF (Fig. 2) also is defined as:

$$y = (\tan\psi_2)x. \tag{6}$$

From the intersection of these two lines, we have:

$$x_2 = \frac{x_1 + \frac{y_1}{\cot\psi_3}}{\frac{\tan\psi_2}{\cot\psi_3} + 1}. \tag{7}$$

Therefore:

$$y_2 = \left(\frac{x_1 + \frac{y_1}{\cot\psi_3}}{\frac{\tan\psi_2}{\cot\psi_3} + 1}\right)\tan\psi_2. \tag{8}$$

Similarly, the equation of line $p_3p_4$ is given by:

$$y - y_4 = -\cot(\psi - \psi_3)(x - x_4), \tag{9}$$

and line OG is defined as:

$$y = x\tan(\psi - \psi_2). \tag{10}$$

Intersecting these two lines, we have:

$$x_3 = \frac{x_4\cot(\psi - \psi_3) + y_4}{\tan(\psi - \psi_2) + \cot(\psi - \psi_3)}. \tag{11}$$

Therefore:

$$y_3 = \left(\frac{x_4\cot(\psi - \psi_3) + y_4}{\tan(\psi - \psi_2) + \cot(\psi - \psi_3)}\right)\tan(\psi - \psi_2). \tag{12}$$

The coordinates of points $p_1$ and $p_4$ are given by:

$$x_1 = x,\ y_1 = x\tan\psi_1 \tag{13}$$

$$x_4 = \frac{x}{\cos\psi_1}\cos(\psi - \psi_1),\ \ y_4 = \frac{x}{\cos\psi_1}\sin(\psi - \psi_1) \tag{14}$$

$$0 \le \psi_1 < \frac{\psi}{2}, \psi_1 < \psi_2 \le \frac{\psi}{2}, 0 \le \psi_3 \le \frac{\psi}{2}. \tag{15}$$

In order to transform the above parameters into dimensionless parameters, use the following:

$$\begin{cases} \frac{x}{h} = u \Rightarrow x = uh \\ \frac{\psi_1}{\frac{\psi}{2}} = v \Rightarrow \psi_1 = \frac{v\psi}{2} \\ \frac{\psi_2}{\frac{\psi}{2}} = w \Rightarrow \psi_2 = \frac{w\psi}{2} \\ \frac{\psi_3}{\frac{\psi}{2}} = r \Rightarrow \psi_3 = \frac{r\psi}{2} \end{cases} \tag{16}$$
$$\frac{b}{h} \le u \le 1, 0 \le v < 1, v < w \le 1, 0 \le r \le 1$$

Now, substituting 16 into 7, 8, 11, 12, 13, and 14, the coordinates of points $P_1$, $P_2$, $P_3$, and $P_4$ are expressed as follows:

$$x_1 = uh \ \ , \ \ y_1 = uh\tan\left(\frac{v\psi}{2}\right) \tag{17}$$

$$x_2 = \frac{x_1 + \frac{y_1}{\cot\left(\frac{r\psi}{2}\right)}}{\frac{\tan\left(\frac{w\psi}{2}\right)}{\cot\left(\frac{r\psi}{2}\right)} + 1} \ \ , \ \ y_2 = x_2\tan\left(\frac{w\psi}{2}\right) \tag{18}$$

$$x_3 = \frac{x_4\cot\left(\left(1 - \frac{r}{2}\right)\psi\right) + y_4}{\tan\left(\left(1 - \frac{w}{2}\right)\psi\right) + \cot\left(\left(1 - \frac{r}{2}\right)\psi\right)} \ \ , \ \ y_3 = x_3\tan\left(\left(1 - \frac{w}{2}\right)\psi\right) \tag{19}$$

$$x_4 = \frac{uh}{\cos\left(\frac{v\psi}{2}\right)}\cos\left(\left(1 - \frac{v}{2}\right)\psi\right) \ \ , \ \ y_4 = \frac{uh}{\cos\left(\frac{v\psi}{2}\right)}\sin\left(\left(1 - \frac{v}{2}\right)\psi\right). \tag{20}$$

Now, a third-degree equation defining the Bezier curve using the above characteristics is defined by Eq. 4. The value of $t$ determines the position of the particle on a streamline.

Using Eqs. 5 and 6, the Cartesian coordinates of the particle are generally defined as:

$$X(t) = x_1(1-t)^3 + 3x_2t(1-t)^2 + 3x_3t^2(1-t) + x_4t^3 \tag{21}$$

$$Y(t) = y_1(1-t)^3 + 3y_2t(1-t)^2 + 3y_3t^2(1-t) + y_4t^3. \tag{22}$$

Now, if in Eqs. 21 and 22 substitutions are made for $x_1$, $y_1$, $x_2$, $y_2$, $x_3$, $y_3$, $x_4$, and $y_4$ from Eqs. 17, 18, 19, and 20, then the coordinates $X$ and $Y$ are defined in terms of $v$, $w$, and $r$. By varying the parameters $v$, $w$, and $r$, the shape of the Bezier curves—Eq. 4—(i.e., the streamlines) could be changed. This means that by varying $v$, $w$, and $r$, the

deforming region changes, and hence, these parameters could later be used in the optimization process.

To formulate a general kinematically admissible velocity field, the method of reference [12] has been modified, the details of which are given in Appendix 1 (see Fig. 3). Therefore, the velocity components for the deforming region of Fig. 2 are given as:

$$\begin{aligned} v_x &= \frac{C}{Y_t X_u - Y_u X_t} X_t \\ v_y &= \frac{C}{Y_t X_u - Y_u X_t} Y_t \end{aligned} \tag{23}$$

where $C$ is given by:

$$C = \frac{v_0 h\left(\cot\left(\frac{r\psi}{2}\right) + \tan\left(\frac{v\psi}{2}\right)\right)\cos\left(\frac{v\psi}{2}\right)\cos\left(\frac{r\psi}{2}\right)}{\cos\left(\frac{r\psi}{2}\right)\cos\left((v-r)\frac{\psi}{2}\right)}. \tag{24}$$

Now, using the above velocity field and the coordinate transformation in Appendix 1 (Eqs. 38, 39, 40, and 41), the strain rate components are readily derived using the following relations:

$$\begin{aligned} \dot{\varepsilon}_x &= \frac{\partial v_x}{\partial x}, \dot{\varepsilon}_y = \frac{\partial v_y}{\partial y} \\ \dot{\tau}_{xy} &= \frac{1}{2}\left(\frac{\partial v_x}{\partial y} + \frac{\partial v_y}{\partial x}\right) \end{aligned} . \tag{25}$$

Using the above strain rate components, the total power for the ECAE process is obtained as follows:

$$\dot{W}_{total} = \dot{W}_i + \dot{W}_{f1} + \dot{W}_{f2} + \dot{W}_{f3} + \dot{W}_l + \dot{W}_{si} + \dot{W}_{so}. \tag{26}$$

The details for computing the different components of the total power have been outlined in Appendix 2. Having calculated the total power for the ECAE process, the extrusion force and pressure are found by:

$$\dot{W}_{total} = F \times v_0. \tag{27}$$

Now the above formulation applies to any metallic material, and if the work hardening behavior of the material

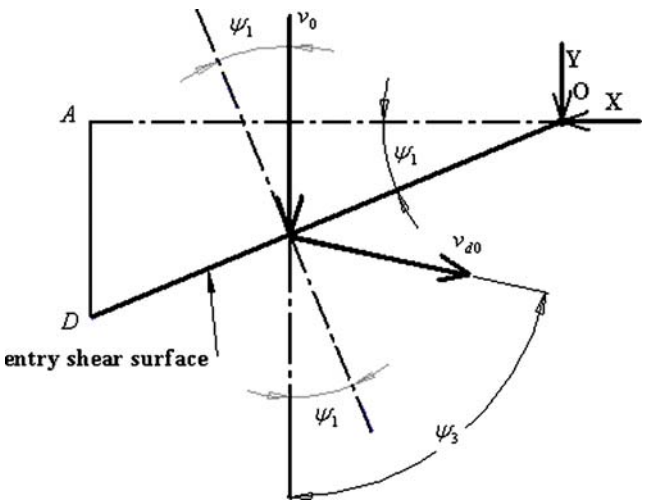


**Fig. 3** Geometry of the entry velocity discontinuity plane

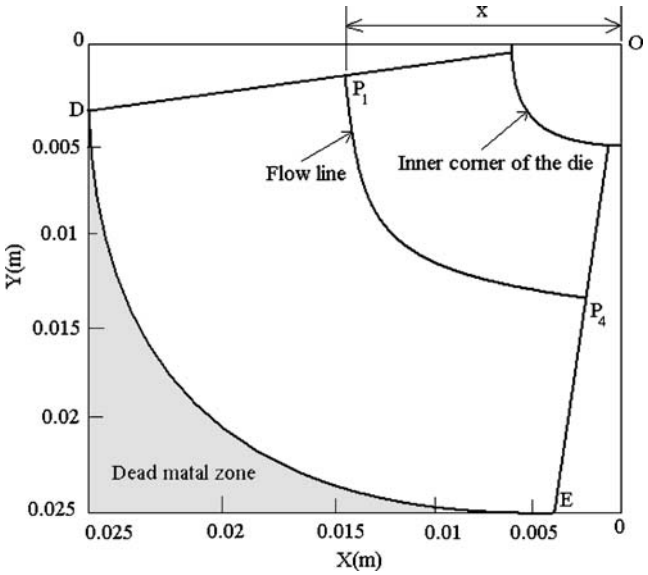


**Fig. 4** Prediction of the dead metal zone and a general streamline

is to be taken into account, then a simple strain hardening rule such as the one given below is used:

$$\overline{\sigma} = k\overline{\varepsilon}^n. \tag{28}$$

To obtain a value for $y_0$ which is used in Appendix 3, the following integration is carried out along a streamline:

$$\overline{y}_0 = \frac{\int_0^{\overline{\varepsilon}_{ave}} \overline{\sigma} d\varepsilon}{\int_0^{\overline{\varepsilon}_{ave}} d\varepsilon} = \frac{\int_0^{\overline{\varepsilon}_{ave}} k\varepsilon^n d\varepsilon}{\overline{\varepsilon}_{ave}}. \tag{29}$$

## 3 Results and discussions

The extrusion of aluminum alloy 2024 was analyzed through a 90° bend die (Fig. 1) using the formulation proposed by the authors. First of all, the shape of the dead metal zone was obtained so that all the surfaces bounding the deforming region were determined. The analysis was carried out using the upper-bound analysis for a typical 90° bend die (Fig. 1) with $a$=0.014$m$ and $b$=0.0005$m$ (Fig. 2). The interface between the dead metal zone and the deforming region as determined by the present analysis is observed in Fig. 4. A typical flow line has also been shown in the same figure.

Theoretical values for normalized extrusion pressure for ECAE through different die angles are shown in Fig. 5 for various frictional conditions. Clearly, as the bend angle becomes steeper, the pressure increases. The behavior of the normalized pressure is linear with respect to die angle values.

Using the present analysis, optimization of the upper-bound results was carried out and the effect of frictional

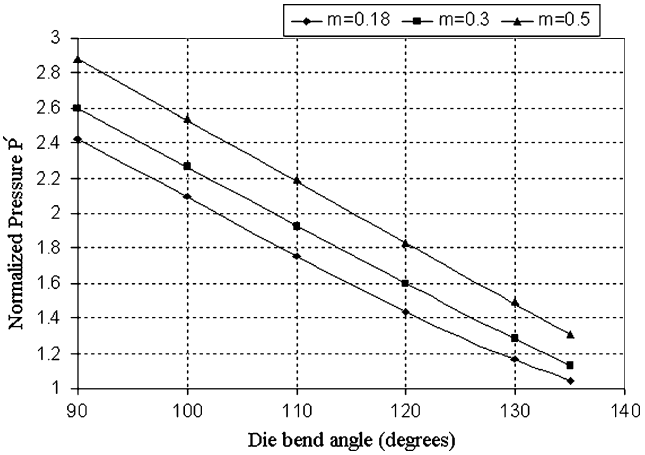


**Fig. 5** Theoretical values for the variations of the normalized extrusion pressure with die angle for different friction factors

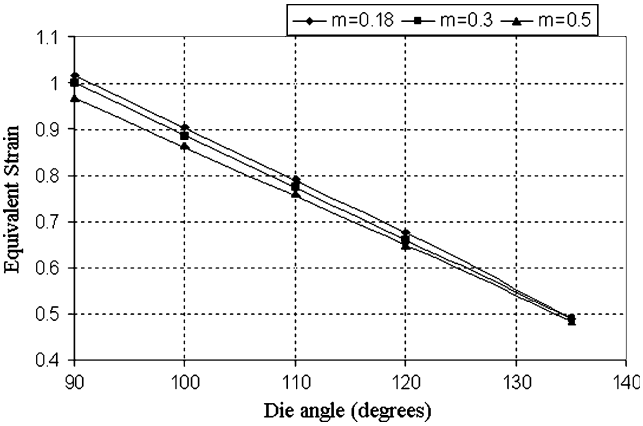


**Fig. 7** Theoretical predictions for the variations of the effective strain with die angle for different friction factors

conditions on the position of the entry velocity discontinuity surface to the deforming region is shown in Fig. 6. These results are shown for different die bend angles. In general, higher friction factors cause the entry velocity discontinuity surface to become more horizontal. For higher die bend angle, the effect of friction on the entry velocity discontinuity was more pronounced. In Fig. 7, the theoretical predictions of the equivalent strains for different die angles could be seen under different frictional conditions. It is clear that frictional conditions do not have great influence on the strain especially at higher die angles. However, for smaller die angles, higher values of strains are obtained. Another interesting result obtained from the analysis was the effect of the frictional conditions on the geometry of deforming region, which is illustrated in Fig. 8. It could be seen that under more severe frictional conditions, the deforming region extends, and as the friction factor decreases, it becomes smaller.

Influence of the internal bend radius of the die on the extrusion pressure and effective strain is shown in Fig. 9.

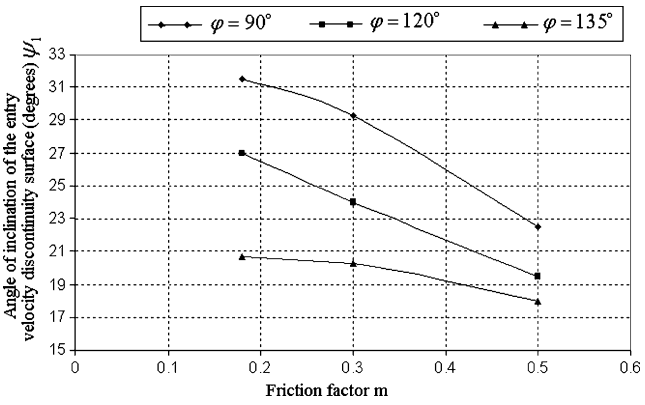


**Fig. 6** Theoretical predictions for the influence of friction on the entry (to the deforming region) velocity discontinuity surface

As far as the normalized extrusion pressure is concerned, sharper bends mean lower pressure, and in general, as the bend radius increases, the normalized pressure increases slightly from about 2.45 for a sharp corner to 3 for a value of $b= 0.02m$. The same trend could be observed for the equivalent strain except that the change in strain is more pronounced as the bend radius increases. This may be explained by the fact that as the bend radius increases, the material has to flow over a bigger surface, thereby expending more energy.

In order to verify the results of the present analysis, experimental results from [1, 2] and [11] have been used. The internal bend radius of the die has been taken as small as possible to simulate a sharp corner. Therefore, the analysis was carried out for a die angle $\phi$=90°, channel length $l$=66 mm, channel width $a$= 14 mm, friction factor, $m$=0.18, material yield strength of 179.3 MPa, and strain hardening exponent $n$=0.26, so the deforming region was obtained as shown in Fig. 10 with DEC as the dead metal

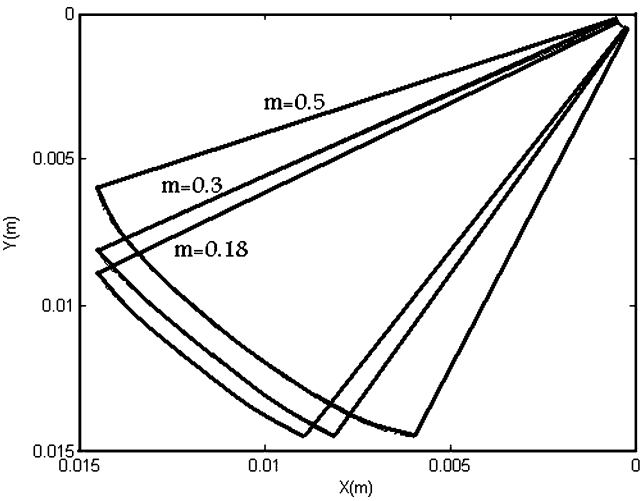


**Fig. 8** Variation of the deforming region with friction factor

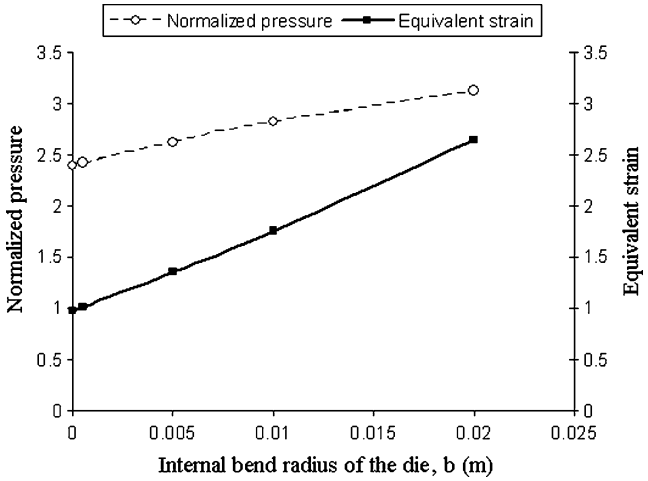


**Fig. 9** Influence of the internal bend radius of the die on the extrusion pressure and effective strain

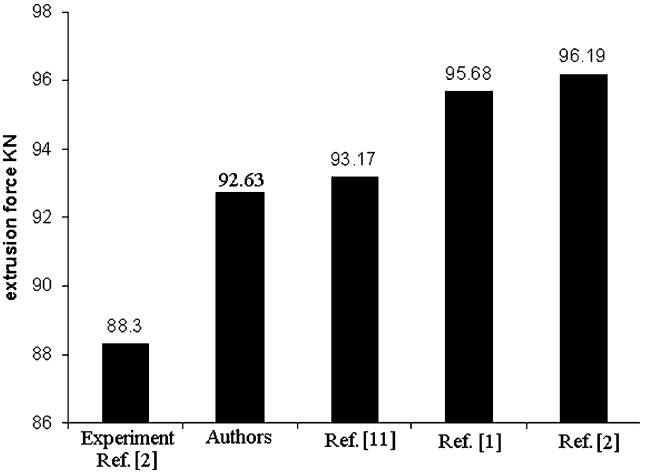


**Fig. 11** Comparison of results for ECAE through a 90° bend die between present theory and previous work

zone. Using these data in Fig. 11, the comparison of authors' results with both experimental and theoretical data from previous work is shown. It could be observed that the results predicted by the present formulations show improvements with regards to previous theoretical work, while it also agrees well with the experimental data.

## 4 Conclusions

A new formulation was developed based on upper-bound theorem for the analysis of ECAE process. This new formulation is more general and much improved with respect to previous work, as it does not make many assumptions and simplifications made in them.

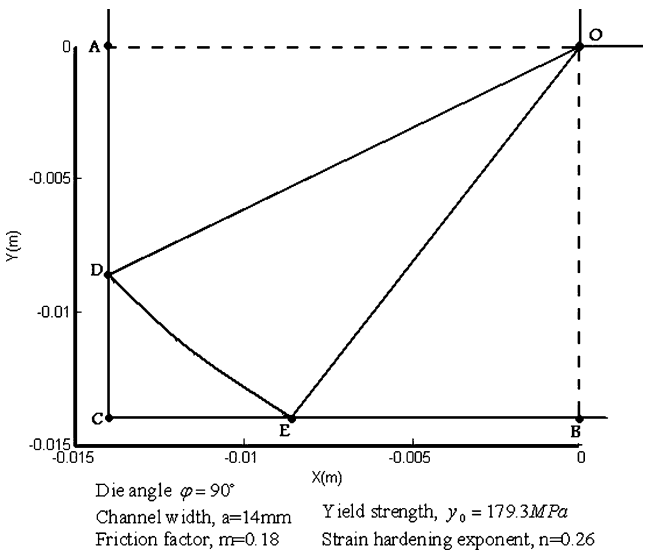


**Fig. 10** Deforming region for the case considered for comparison of results

The deforming region was defined in a general way so that when minimizing the upper bound, the shape of the deforming region was optimized to become as close as possible to the real situation. This general definition of the deforming region gave this formulation an advantage over previous work which had used fixed deforming regions.

By the optimization process of the upper-bound formulation, the shape of the dead metal zone was predicted and the effect of friction simulated. Again, in the formulation presented here, a generalized Bezier curve was taken for the boundary of the dead metal zone, while in previous work, a circular boundary was assumed.

The relative extrusion pressure computed from the present theory was yet the closest to the experimental data as compared with previous works.

Using the present formulation, a die design (bend angle, inner and outer bend radius) was obtained where larger strains were experienced in one pass, while the increase in the extrusion pressure was not significant.

## Appendix 1

A general kinematically admissible velocity field

With reference to [12] and considering that in this paper a plane strain deformation has been assumed, the equation of the tangent at a general point in the deforming region is defined by:

$$\vec{r}_t = X_t\vec{i} + Y_t\vec{j}. \tag{30}$$

Since this point is placed on a streamline (see Fig. 2), then its velocity is defined by:

$$\vec{v} = v_x\vec{i} + v_y\vec{j}. \tag{31}$$

The two vectors are parallel, which means:

$$\frac{v_x}{X_t} = \frac{v_y}{Y_t} \Rightarrow v_x = \frac{X_t}{Y_t} v_y. \tag{32}$$

The above equation should satisfy the condition for incompressibility:

$$\frac{\partial v_x}{\partial x} + \frac{\partial v_y}{\partial y} = 0. \tag{33}$$

On the other hand, since $X$ and $Y$ are defined in terms of $u$ and $t$, then the following transformation should be used to obtain the velocity components:

$$\begin{bmatrix} \frac{\partial v_x}{\partial x} & \frac{\partial v_x}{\partial y} \\ \frac{\partial v_y}{\partial x} & \frac{\partial v_y}{\partial y} \end{bmatrix} = \begin{bmatrix} \frac{\partial v_x}{\partial u} & \frac{\partial v_x}{\partial t} \\ \frac{\partial v_y}{\partial u} & \frac{\partial v_y}{\partial t} \end{bmatrix} \times \begin{bmatrix} \frac{\partial u}{\partial x} & \frac{\partial u}{\partial y} \\ \frac{\partial t}{\partial x} & \frac{\partial t}{\partial y} \end{bmatrix}. \tag{34}$$

Using the determinant $j$ and its inverse, we have:

$$j = \begin{bmatrix} X_u & X_t \\ Y_u & Y_t \end{bmatrix} \tag{35}$$

$$j^{-1} = \begin{bmatrix} \frac{\partial u}{\partial x} & \frac{\partial u}{\partial y} \\ \frac{\partial t}{\partial x} & \frac{\partial t}{\partial y} \end{bmatrix}. \tag{36}$$

Hence, the following expression is obtained:

$$\begin{bmatrix} \frac{\partial v_x}{\partial x} & \frac{\partial v_x}{\partial y} \\ \frac{\partial v_y}{\partial x} & \frac{\partial v_y}{\partial y} \end{bmatrix} = \frac{1}{\det j} \begin{bmatrix} \frac{\partial v_x}{\partial u} & \frac{\partial v_x}{\partial t} \\ \frac{\partial v_y}{\partial u} & \frac{\partial v_y}{\partial t} \end{bmatrix} \times \begin{bmatrix} Y_t & -X_t \\ -Y_u & X_u \end{bmatrix}. \tag{37}$$

Therefore, from 37, the following components for the derivatives of the velocity components are derived:

$$\frac{\partial v_x}{\partial x} = \frac{1}{\det j}\left(\frac{\partial v_x}{\partial u} Y_t - \frac{\partial v_x}{\partial t} Y_u\right) \tag{38}$$

$$\frac{\partial v_x}{\partial y} = \frac{1}{\det j}\left(-\frac{\partial v_x}{\partial u} X_t + \frac{\partial v_x}{\partial t} X_u\right) \tag{39}$$

$$\frac{\partial v_y}{\partial x} = \frac{1}{\det j}\left(\frac{\partial v_y}{\partial u} Y_t - \frac{\partial v_y}{\partial t} Y_u\right) \tag{40}$$

$$\frac{\partial v_y}{\partial y} = \frac{1}{\det j}\left(-\frac{\partial v_y}{\partial u} X_t + \frac{\partial v_y}{\partial t} X_u\right). \tag{41}$$

Using the above components and substituting in the incompressibility, Eq. 3333 yields:

$$Y_t \frac{\partial v_x}{\partial u} - Y_u \frac{\partial v_x}{\partial t} - X_t \frac{\partial v_y}{\partial u} + X_u \frac{\partial v_y}{\partial t} = 0. \tag{42}$$

Simplifying, we have:

$$Y_t\left(\frac{\left(X_{tu} v_y + X_t v_{yu}\right) Y_t - Y_{tu} X_t v_y}{Y_t^2}\right) - Y_u\left(\frac{\left(X_{tt} v_y + X_t v_{yt}\right) Y_t - Y_{tt} X_t v_y}{Y_t^2}\right) - X_t v_{yu} + X_u v_{yt} = 0. \tag{43}$$

Rearranging the above expression gives:

$$\underbrace{\left(X_{tu} - \frac{Y_{tu}}{Y_t} X_t - \frac{Y_u}{Y_t} X_{tt} + \frac{Y_u}{Y_t^2} Y_{tt} X_t\right)}_{A} v_y + \underbrace{\left(X_u - \frac{Y_u}{Y_t} X_t\right)}_{B} \frac{\partial v_y}{\partial t} = 0. \tag{44}$$

Hence, the following simple expression is obtained, expressing 44 as:

$$A v_y + B \frac{\partial v_y}{\partial t} = 0. \tag{45}$$

Noting that:

$$A = \frac{\partial B}{\partial t} \tag{46}$$

Then 45 is rewritten as:

$$\frac{\partial B}{\partial t} v_y + B \frac{\partial v_y}{\partial t} = 0. \tag{47}$$

Rearranging 47 yields:

$$\frac{\partial v_y}{v_y} = -\frac{\partial B}{B}. \tag{48}$$

Integrating 48 gives:

$$\ln\left(v_y\right) = -\ln(B) + \ln C = \ln\left(\frac{C}{B}\right) \tag{49}$$

where

$$v_y = \frac{C}{B} \tag{50}$$

$$B = X_u - \frac{Y_u}{Y_t} X_t. \tag{51}$$

*Velocity discontinuities at entry and exit*: Considering Fig. 3, the direction of the initial velocity, $\nu_0$, changes after entering the deforming region by an amount of $\psi_3$, and its magnitude becomes $\nu_{d0}$. By equating the components of the velocity perpendicular to the shear plane $DD'$, we have:

$$v_{d0}\cos(\psi_3 - \psi_1) = v_0 \cos\psi_1 \Rightarrow v_{\mathrm{d0}} = \frac{v_0 \cos\psi_1}{\cos(\psi_3 - \psi_1)} \Rightarrow v_{\mathrm{d0}} = \frac{v_0 \cos\left(\frac{v\psi}{2}\right)}{\cos\left((r - v)\frac{\psi}{2}\right)}. \tag{52}$$

The components of $\nu_{d0}$ in $x$ and $y$ directions are:

$$v_{d0x} = -\frac{v_0 \cos\left(\frac{v\psi}{2}\right)}{\cos\left((r-v)\frac{\psi}{2}\right)} \sin\left(\frac{r\psi}{2}\right) \tag{53}$$

$$v_{d0y} = \frac{v_0 \cos\left(\frac{v\psi}{2}\right)}{\cos\left((r-v)\frac{\psi}{2}\right)} \cos\left(\frac{r\psi}{2}\right). \tag{54}$$

Therefore, the velocity discontinuity along $DD'$ is given by:

$$|\Delta v| = \left| \frac{v_0 \cos\left(\frac{v\psi}{2}\right)}{\cos\left((r-v)\frac{\psi}{2}\right)} \sin\left((r-v)\frac{\psi}{2}\right) + v_0 \sin\left(\frac{v\psi}{2}\right) \right|. \tag{55}$$

Considering Eq. 50 yields:

$$\begin{cases} t=0 \Rightarrow v_y = v_{d0y} \\ t=0 \Rightarrow B = B_{t=0} \end{cases} \Rightarrow v_y = \frac{C}{B}. \tag{56}$$

Hence, a value is obtained for $C$ as follows:

$$C = \frac{v_0 h \left(\cot\left(\frac{r\psi}{2}\right) + \tan\left(\frac{v\psi}{2}\right)\right) \cos\left(\frac{v\psi}{2}\right) \cos\left(\frac{r\psi}{2}\right)}{\cot\left(\frac{r\psi}{2}\right) \cos\left((v-r)\frac{\psi}{2}\right)}. \tag{57}$$

Note that in case of no velocity discontinuity, $r=0 \Rightarrow C=h\nu_0$.

Therefore, by substituting 5757 and 51 into 50, the general kinematically admissible velocity field is obtained as follows:

$$v_x = \frac{C}{Y_t X_u - Y_u X_t} X_t \tag{58}$$

$$v_y = \frac{C}{Y_t X_u - Y_u X_t} Y_t. \tag{59}$$

Note that no matter what the deforming region is, the general velocity field is always automatically admissible. This would be a great help when optimizing the upper-bound solution.

## Appendix 2

Components of the ECAE total power

Having obtained the velocity and strain rate fields, the components of the ECAE total power are determined as follows:

The power of internal deformation:

$$\begin{cases} \dot{W}_i = \frac{2y_0 a}{\sqrt{3}} \int_{\frac{b}{h}}^{1} \int_{0}^{1} \left[ \left( \frac{\dot{\varepsilon}_x^2 + \dot{\varepsilon}_y^2}{2} \right) + \dot{\varepsilon}_{xy}^2 \right]^{\frac{1}{2}} \left| \frac{\partial(x,y)}{\partial(u,t)} \right| \mathrm{dtdu}. \\ \left| \frac{\partial(x,y)}{\partial(u,t)} \right| = \left| \begin{matrix} \frac{\partial X}{\partial u} & \frac{\partial Y}{\partial u} \\ \frac{\partial X}{\partial t} & \frac{\partial Y}{\partial t} \end{matrix} \right| = X_u Y_t - Y_u X_t \end{cases} \tag{60}$$

The component of power due to the shear at the interface of the dead metal zone and the deforming region is given by:

$$\dot{W}_{f1} = \iint \tau_f |\Delta v| \mathrm{ds} = \frac{\mathrm{my}_0}{\sqrt{3}} \iint \left( \mathrm{v}_\mathrm{x}^2 + \mathrm{v}_\mathrm{y}^2 \right)^{\frac{1}{2}} |_{\mathrm{u}=1} \mathrm{ds} \tag{61}$$

where

$$\mathrm{ds} = \mathrm{a} \frac{\mathrm{dy}}{\cos\alpha}. \tag{62}$$

By substituting 62 into 61 and coordinate transformation:

$$\dot{W}_{f1} = \frac{m y_0 a}{\sqrt{3}} \int_0^1 \left( v_x^2 + v_y^2 \right)^{\frac{1}{2}} |_{u=1} \frac{1}{\cos\alpha} Y_t \mathrm{dt} \tag{63}$$

where

$$\frac{1}{\cos\alpha} = \frac{1}{\vec{T} \times \vec{j}}. \tag{64}$$

Here, $\vec{T}$ is the tangent vector to the streamline given by:

$$T(t) = \frac{1}{\left(X_t^2 + Y_t^2\right)^{\frac{1}{2}}} \left( X_t \vec{i} + Y_t \vec{j} \right). \tag{65}$$

Therefore,

$$\frac{1}{\cos\alpha} = \frac{\left(X_t^2 + Y_t^2\right)^{\frac{1}{2}}}{Y_t}. \tag{66}$$

Now, substituting 66 into 63 and considering $m=1$ for the interface of the deforming region and the dead metal zone, the component of power dissipated due to the dead metal zone interface with the deforming region is given by:

$$\dot{W}_{\mathrm{f1}} = \frac{y_0 a}{\sqrt{3}} \int_0^1 \left( v_x^2 + v_y^2 \right)^{\frac{1}{2}} |_{u=1} \left( X_t^2 + Y_t^2 \right)^{\frac{1}{2}} |_{u=1} \mathrm{dt}. \tag{67}$$

The component of power due to velocity discontinuity at the inner surface of the die (Fig. 2) is given by:

$$\dot{W}_{f2} = \frac{m y_0 a}{\sqrt{3}} \int_0^1 \left( v_x^2 + v_y^2 \right)^{\frac{1}{2}} \Big|_{u=\frac{b}{h}} \left( X_t^2 + Y_t^2 \right)^{\frac{1}{2}} \Big|_{u=\frac{b}{h}} \mathrm{dt} \tag{68}$$

where

$$\tau_0 = \frac{y_0}{\sqrt{3}}.$$

The component of power due to velocity discontinuity at the interface of the deforming region and the die (Fig. 2)—interfaces $AD$ and $EB$—is given by:

$$\dot{W}_{f3} = 2(m\tau_0 v_0 h \tan\psi_1 a) = 2m\tau_0 v_0 h a \tan\left(\frac{v\psi}{2}\right). \tag{69}$$

The components of power due to velocity discontinuity at the interfaces of the rigid material region and the die (Fig. 2)—before and after $AA'$ and $BB'$ where the material moves in a rigid fashion on the die surface—are given by:

$$\begin{aligned}\dot{W}_l(\mathrm{i}) &= 4ma\tau_0 v_0 l_\mathrm{i}\\ \dot{W}_l(\mathrm{o}) &= 4ma\tau_0 v_0 l_o.\end{aligned} \tag{70}$$

The components of power due to velocity discontinuity at entry ($DD'$) and exit surfaces ($EE'$) of the deforming region (Fig. 2) are given by:

$$\dot{W}_{si} = \dot{W}_{so} = \tau_0|\Delta v|\mathrm{ds} = \frac{\mathrm{ay}_0}{\sqrt{3}}\int|\Delta \mathrm{v}|\mathrm{dl}. \tag{71}$$

Now, considering Fig. 2, note that:

$$\begin{aligned}\mathrm{dl}\cos\psi_1 &= \mathrm{dx}\\ \mathrm{dl} &= \tfrac{\mathrm{dx}}{\cos\psi_1} = \tfrac{\mathrm{dx}}{\cos\left(\frac{v\psi}{2}\right)}.\end{aligned} \tag{72}$$

For point $p_1$ in the shear surface $DD'$, we have:

$$x = uh \Rightarrow dx = hdu. \tag{73}$$

Substituting 73 into 72 gives:

$$\mathrm{dl} = \frac{\mathrm{hdu}}{\cos\left(\frac{\mathrm{v}\psi}{2}\right)}. \tag{74}$$

Substituting 74 into 71 yields:

$$\dot{W}_{si} = \dot{W}_{so} = \frac{ay_0}{\sqrt{3}}\int_{\frac{b}{h}}^{1}|\Delta v|\frac{hdu}{\cos\left(\frac{v\psi}{2}\right)}. \tag{75}$$

Substituting 55 into 75 and integrating gives:

$$\dot{W}_\mathrm{s} = \dot{W}_{si} + \dot{W}_{so} = \frac{2}{\sqrt{3}}ahy_0v_0\left(1-\frac{b}{h}\right)\left(\tan\left((r-v)\frac{\psi}{2}\right)+\tan\left(\frac{v\psi}{2}\right)\right). \tag{76}$$

## Appendix 3

Average strain

The equivalent or effective strain rate, in general, is defined as:

$$\bar{\dot{\varepsilon}} = \frac{2}{\sqrt{3}}\sqrt{\frac{1}{2}\dot{\varepsilon}_{ij}\dot{\varepsilon}_{ij}} = \frac{2}{\sqrt{3}}\left(\frac{\dot{\varepsilon}_x^2+\dot{\varepsilon}_y^2+\dot{\varepsilon}_z^2+2\dot{\varepsilon}_{xy}^2+2\dot{\varepsilon}_{xz}^2+2\dot{\varepsilon}_{yz}^2}{2}\right). \tag{77}$$

For the plane strain deformation, we have:

$$\bar{\dot{\varepsilon}} = \frac{2}{\sqrt{3}}\left(\frac{\dot{\varepsilon}_x^2+\dot{\varepsilon}_y^2}{2}+\dot{\varepsilon}_{xy}^2\right)^{\frac{1}{2}}. \tag{78}$$

*Equivalent strain in the deforming region*: The effective strain is determined by integrating 78 with respect to time:

$$\bar{\varepsilon} = \int\bar{\dot{\varepsilon}}\mathrm{dt}. \tag{79}$$

Taking an element of distance d$s$ on the streamline, the velocity of a particle passing through that distance is given by: $\frac{\mathrm{ds}}{\mathrm{dt}} = v$ where $\mathrm{ds}\cos\alpha = \mathrm{dy}$ and $\frac{1}{\cos\alpha} = \frac{\left(X_t^2+Y_t^2\right)^{\frac{1}{2}}}{Y_t}$ hence:

$$\mathrm{dt} = \frac{1}{\mathrm{v}}\frac{1}{\cos\alpha}\mathrm{dy} = \frac{\left(\mathrm{X_t^2+Y_t^2}\right)^{\frac{1}{2}}}{\mathrm{Y_t}\left(\mathrm{v_x^2+v_y^2}\right)^{\frac{1}{2}}}\mathrm{dy}. \tag{80}$$

Substituting 78 and 80 into 79 yields:

$$\bar{\varepsilon} = \frac{2}{\sqrt{3}}\int\left(\frac{\dot{\varepsilon}_x^2+\dot{\varepsilon}_y^2}{2}+\dot{\varepsilon}_{xy}^2\right)^{\frac{1}{2}}\frac{\left(X_t^2+Y_t^2\right)^{\frac{1}{2}}}{Y_t\left(v_x^2+v_y^2\right)^{\frac{1}{2}}}\mathrm{dy}. \tag{81}$$

Changing d$y$ into d$t$ gives:

$$\bar{\varepsilon} = \frac{2}{\sqrt{3}}\int_0^1\left(\frac{\dot{\varepsilon}_x^2+\dot{\varepsilon}_y^2}{2}+\dot{\varepsilon}_{xy}^2\right)^{\frac{1}{2}}\frac{\left(X_t^2+Y_t^2\right)^{\frac{1}{2}}}{Y_t\left(v_x^2+v_y^2\right)^{\frac{1}{2}}}Y_t\mathrm{dt}. \tag{82}$$

Finally simplifying, the strain induced in the deforming region is given by:

$$\bar{\varepsilon}_{\mathrm{stream}} = \bar{\varepsilon} = \frac{2}{\sqrt{3}}\int_0^1\left(\frac{\dot{\varepsilon}_x^2+\dot{\varepsilon}_y^2}{2}+\dot{\varepsilon}_{xy}^2\right)^{\frac{1}{2}}\frac{\left(X_t^2+Y_t^2\right)^{\frac{1}{2}}}{\left(v_x^2+v_y^2\right)^{\frac{1}{2}}}\mathrm{dt}. \tag{83}$$

*Strain induced at entry and exit discontinuity surfaces*: In the entry and exit shear surfaces, there are some strains which are obtained by dividing the velocity discontinuity by the perpendicular component of the velocity to the shear surface as follows:

$$\gamma_i = \gamma_0 = \frac{|\Delta v|}{v_0\cos\psi_1} = \frac{|\Delta v|}{v_0\cos\left(\frac{v\psi}{2}\right)} = \left|\tan\left((r-v)\frac{\psi}{2}\right)+\tan\left(\frac{v\psi}{2}\right)\right| \tag{84}$$

where $\gamma_i$ and $\gamma_0$ are the shear strains in surfaces $E'E$ and $D'D$. The equivalent strain is therefore given by:

$$\varepsilon_{si} = \varepsilon_{so} = \frac{1}{\sqrt{3}}\left|\tan\left((r-v)\frac{\psi}{2}\right)+\tan\left(\frac{v\psi}{2}\right)\right|. \tag{85}$$

Hence, the total strain induced in the material is given by:

$$\bar{\varepsilon}_{ave} = \bar{\varepsilon}_\mathrm{s} + \bar{\varepsilon}_{stream}. \tag{86}$$

## References


1. Altan BS, Purcek G, Miskioglu I (2005) An upper-bound analysis for equal-channel angular extrusion. J Mater Process Technol 168:137–146
2. Eivani AR, Karimi Taheri A (2007) An upper bound solution of ECAE process with outer curved corner. J Mater Process Technol 182:555–563. doi:10.1016/j.jmatprotec.2006.09.021
3. Sandim HRZ, Bernardi HH, Verlinden B, Raabe D (2007) Equal channel angular extrusion of niobium single crystals. Mater Sci Eng A 467:44–52. doi:10.1016/j.msea.2007.02.086
4. Li A, Gazder SA, Beyerlein IJ, Davies CHJ, Pereloma EV (2007) Microstructure and texture evolution during equal channel angular extrusion of interstitial-free steel: effects of die angle and processing route. Acta Mater 55:1017–1032. doi:10.1016/j.actamat.2006.09.022
5. Zhang ZJ, Son IH, Im YT, Park JK (2007) Finite element analysis of plastic deformation of CP-Ti by multi-pass equal channel angular extrusion at medium hot-working temperature. Mater Sci Eng A 447:134–141. doi:10.1016/j.msea.2006.10.068
6. Tham YW, Fu MW, Hng HH, Yong MS, Lim KB (2007) Bulk nanostructured processing of aluminum alloy. J Mater Process Technol 192–193:575–581. doi:10.1016/j.jmatprotec.2007.04.076
7. Petryk H, Stupkiewicz S (2007) A quantitative model of grain refinement and strain hardening during severe plastic deformation. Mater Sci Eng A 444:214–219. doi:10.1016/j.msea.2006.08.076
8. Kecskes LJ, Cho KC, Dowding RJ, Schuster BE, Valiev RZ, Wei Q (2007) Grain size engineering of bcc refractory metals: top-down and bottom-up—application to tungsten. Mater Sci Eng A 467:33–43. doi:10.1016/j.msea.2007.02.099
9. Su CW, Lu L, Lai MO (2006) A model for the grain refinement mechanism in equal channel angular pressing of Mg alloy from microstructural studies. Mater Sci Eng A 434:227–236. doi:10.1016/j.msea.2006.06.103
10. Hasani A, Lapovok R, To'th LS, Molinari A (2008) Deformation field variations in equal channel angular extrusion due to back pressure. Scr Mater 58:771–774. doi:10.1016/j.scriptamat.2007.12.018
11. Eivani AR, Karimi Taheri A (2008) The effect of dead metal zone formation on strain and extrusion force during equal channel angular extrusion. Comput Mater Sci 42:14–20. doi:10.1016/j.commatsci.2007.06.001
12. Abrinia K, Bloorbar H (2000) A new improved upper bound solution for the extrusion of shaped sections using CAD techniques. COMPLAS VI Conference, Barcelona, Spain